N91-10460

LIDAR AND AIRCRAFT STUDIES OF DEEP CIRRUS SYSTEMS FROM THE 1986 FIRE IFO

K. Sassen

Meteorology Department
University of Utah
Salt Lake City, Utah 84112

A. Heymsfield and N. Knight

National Center for Atmospheric Research*
Boulder, Colorado 80307

Several NCAR King Air flight missions were conducted during the Wisconsin FIRE IFO experiment in support of University of Utah polarization lidar observations of deep cirrus cloud systems at the Wausau ground site. Data collected from four cirrus systems are included in this analysis, including those of 22 and 28 October, and 1 and 2 November. Lidar data were generally obtained at 2-min intervals in the zenith direction over observation periods that ranged from ~4 to 10 h, bracketing the aircraft missions. The data have been processed to yield height-time (HTI) displays of lidar linear depolarization ratio δ and relative range-normalized returned power P. King Air operations consisted of a combination of rapid profiling and Lagrangian spiral descents and stacked race-track patterns (flown approximately along the cirrus level wind direction) in the vicinity of the field site. From the spiral descents are constructed vertical profiles of ice particle ($\geq$75 μm) concentration N_i and ice mass content IWC derived from PMS 2D-probe imagery and, when detected, FSSP cloud droplet concentration N_w and liquid water content LWC. Aircraft flight leg data are presented for vertical velocity W and the same ice and water cloud content parameters. In addition, aerosol particle concentrations (0.1-3.0 μm) obtained with the ASAS probe are examined, and photographs of ice particles collected in situ on oil-coated slides are presented to illustrate ice particle habit.

As an example of a partial dataset from a deep cirrus cloud system, we present for the 1 November 1986 case study, HTI displays of lidar relative (range-normalized) returned laser power and δ values (bottom of Fig. 1, see caption), and aircraft temperature, ice mass content and crystal concentration vertical profiles obtained during two spiral descents through the cloud (Fig. 2). The altitude of the aircraft over the ground site during the mission is shown in the displays as the solid line, and the times that the ice crystal slide samples given in Fig. 3 were obtained are depicted by the circles. The position of the aircraft generally remained within 15 km of the ground site during the period shown in Fig. 1.

---

*The National Center for Atmospheric Research is supported by the National Science Foundation.

PRECEDING PAGE BLANK NOT FILMED

The cloud structure on 1 November is similar to that of the three other deep cirrus cloud systems in that altocumulus layers containing supercooled liquid were connected with the cirrus development at low levels. As indicated at the beginning of the data display of Fig. 1, the relatively low $\delta \leq 0.15$ values (filled-in) and enhanced returns that occur just above the frontal inversion at 5.3 km (-19°C) reveal the presence of supercooled cloud droplets. Below the altocumulus is a thin virga layer, which often appears to be composed of horizontally oriented plate crystals. Although dense cirrus is initially present above 7.5 km, the region immediately above the altocumulus appears to be cloud free until ~1830, when ice particles precipitating from the cirrus reach cloud base. This precipitation trail contains strong laser returns and the relatively high $\delta \approx 0.5$ values indicative of complex ice crystals or aggregates. Subsequently, a series of additional precipitation trails generated within the upper level cirrus provide a more or less continuous supply of ice particles to the newly established cirrus cloud base, which develops into a strongly scattering layer. Clearly, the cloud generation processes responsible for the thin altocumulus were also responsible for the development of the dense cirrus cloud base layer, once sufficiently strong cirrus particle precipitation occurred to humidify and breach the intervening cloud free layer.

Aircraft microphysical data from the first spiral descent (Fig. 2a) show relatively high particle concentrations within an upper cirrus level generating region above ~8 km (see top of Fig. 1), and variable concentrations below ~7 km. In terms of ice mass content, a gradual increase in IWC is present with decreasing height in the lower cloud region, with the peak occurring at the 5.3 km level formerly occupied by the altocumulus layer. The photomicrographs of Fig. 3 reveal that the strongly scattering cloud base region displaying $\delta \approx 0.5$ values contained complex, hollow column crystals. During the second spiral descent (Fig. 2b), ice crystal concentrations decrease slightly, while IWC values tend to increase. The IWC ≥ 0.01 g m^{-3} values present between 5.3-7.4 km correspond to a layer of strong laser returns and $\delta \approx 0.5$ values, which produced sufficient optical attenuation to have limited the lidar detection of the upper cirrus cloud region at that time.

The vertical profiles of IWC obtained during both spiral descents suggest that ice particle aggregation was occurring within the deep cirrus. On the basis of the lidar data, ice crystal production appears to have occurred primarily within the generating regions near cloud tops, and also within the occasionally water-saturated cloud base region. Further analyses are underway to obtain more detailed knowledge of the effects of the aggregation process.

Acknowledgments. This research has been supported primarily by Grant ATM-85 13975 from the National Science Foundation and by NASA project order #L-08100B.

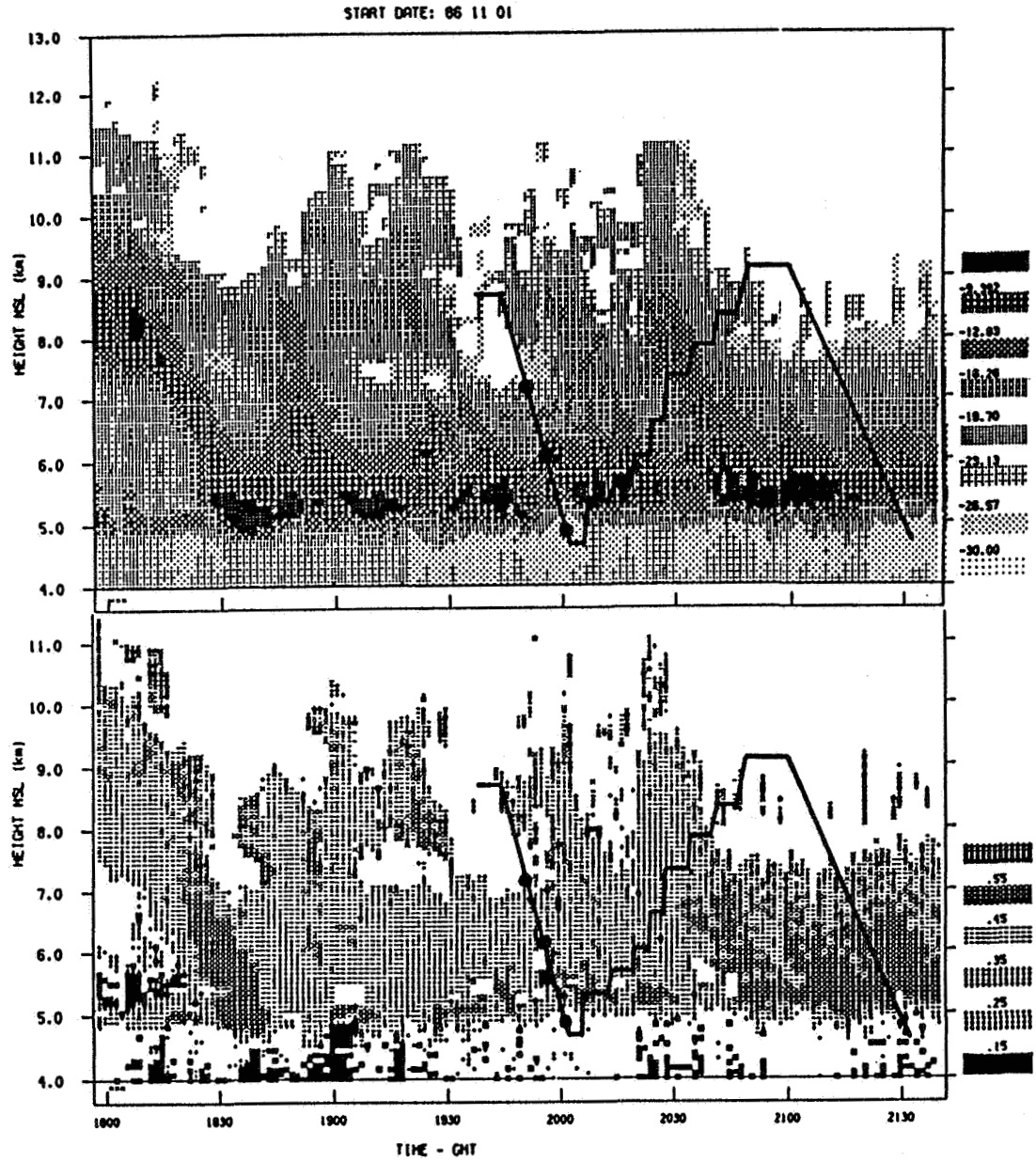

Fig. 1 Height-time displays of lidar relative returned laser power in dB of the maximum range-normalized signal (top, note gray scale at right) and linear depolarization ratio (bottom, with δ value scale at right) for the 1 November 1986 FIRE IFO cirrus cloud system. The approximate position of the King Air aircraft in the vicinity of the Wausau ground site is shown by the lines for the two spirals and stepped ascent ramps, where the circles represent the ice crystal slide samples given in Fig. 3.

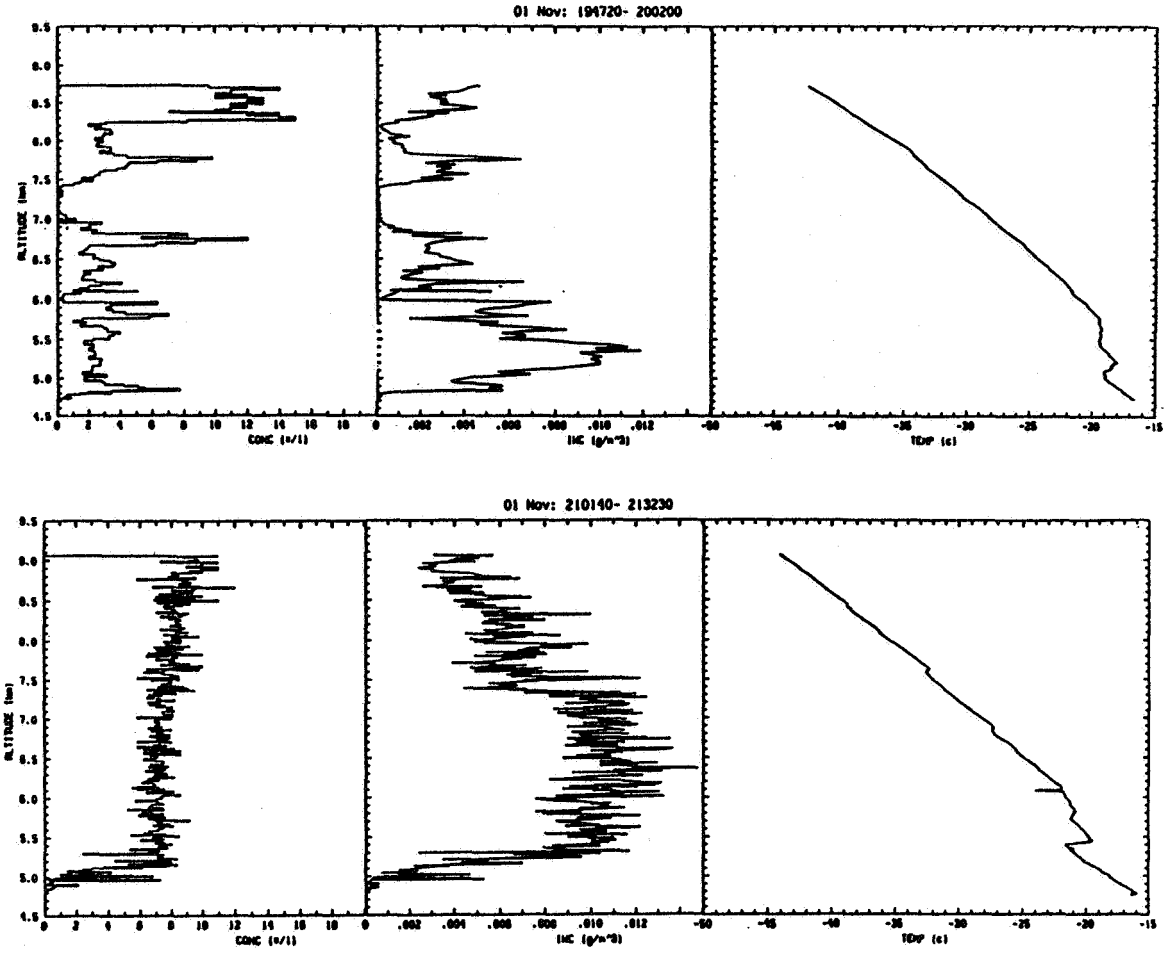

Fig. 2 Aircraft microphysical and temperature profiles obtained during the two spiral descents shown in Fig. 1. Given are the concentrations of ice crystals (per liter) and the ice mass content IWC (g m^{-3}) derived from PMS 2D-probe imagery.

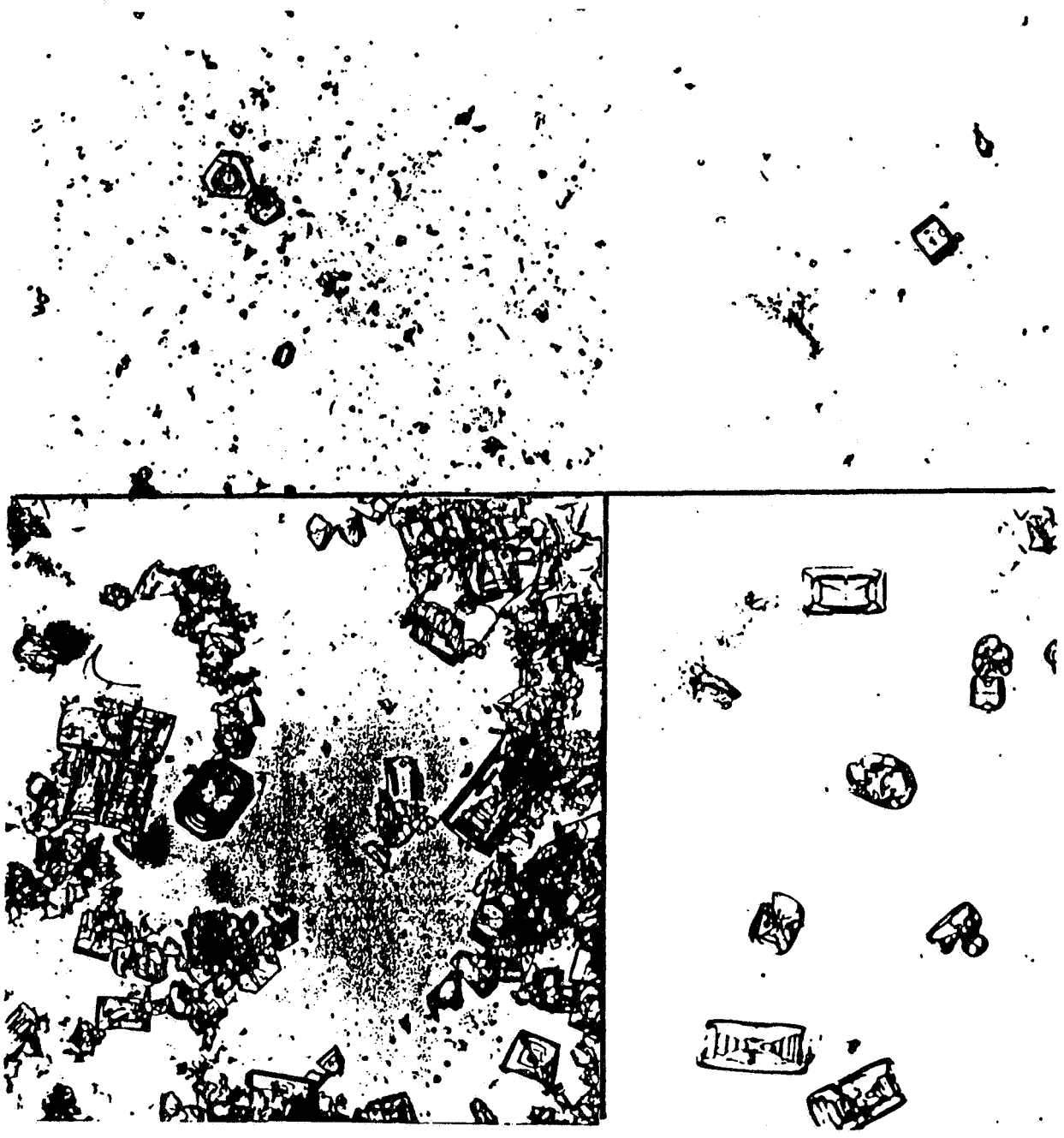

Fig. 3 Photomicrographs of ice crystals collected on three slides during the first aircraft spiral. At top are short column and thick plate crystals from a thin ice cloud at 7.15 km (-29.3°C); at bottom left are hollow columns displaying considerable internal structure from the lower cloud region at 6.15 km (-21.9°C); and at bottom right are hollow columns with rounded edges and a loss of internal structure due to evaporation, from 4.84 km (-17.6°C). The loss of crystalline scattering properties from evaporation typically causes lidar δ values to decrease at cloud base (see Fig. 1).